



Lithium diffusion in olivine records magmatic priming of explosive basaltic eruptions

Kendra J. Lynn^{a,b,*}, Thomas Shea^a, Michael O. Garcia^a, Fidel Costa^c, Marc D. Norman^d

^a Department of Geology and Geophysics, University of Hawai'i, Honolulu, HI 96822, USA

^b Department of Geological Sciences, University of Delaware, Newark, DE 19716, USA

^c Earth Observatory of Singapore, Asian School of the Environment, Nanyang Technological University, 639798, Singapore, Singapore

^d Research School of Earth Sciences, Australian National University, Canberra, ACT 0200, Australia

ARTICLE INFO

Article history:

Received 2 March 2018

Received in revised form 31 July 2018

Accepted 2 August 2018

Available online 22 August 2018

Editor: T.A. Mather

Keywords:

olivine
diffusion
lithium zoning
Kilauea
Hawai'i

ABSTRACT

The short duration (e.g., hours to days) of magmatic processes leading up to volcanic eruptions are challenging to characterize using conventional petrologic and geophysical methods. This is especially true for eruptions that occurred prior to the implementation of seismic and geodetic monitoring (mid-20th century). We present a new application of diffusion chronometry that utilizes lithium zoning in olivine phenocrysts to investigate the timing of late-stage, pre-eruptive magma mixing at Kilauea Volcano (Hawai'i). The diffusive re-equilibration of sub-ppm changes in lithium concentration are modeled in rapidly quenched, well-oriented olivine from six eruptions during a dominantly explosive period (1500–1820 CE). Lithium timescales reveal repeated intrusion of primitive composition magma into Kilauea's shallow (~2–6 km) reservoir system typically only a few days prior to each eruption. These timescales are shorter than the weeks to years retrieved from modeling Fe–Mg and Ni zoning in the same olivine crystals, which record earlier magma mixing events. The short Li timescales indicate that an intrusion primed the shallow magma reservoir potentially only hours to a few days before an eruption. Late-stage intrusions and mixing events should thus be investigated at other basaltic volcanoes to better understand pre-eruptive processes, so that eruption scenarios can be better constrained.

© 2018 Elsevier B.V. All rights reserved.

1. Introduction

1.1. Priming volcanic eruptions

A fundamental challenge of mitigating volcanic hazards is identifying the magmatic processes that occur right before eruptions (National Academies of Sciences, Engineering, and Medicine, 2017). The timing of such events is often difficult to detect and characterize with current geophysical, petrologic and geochemical methods (e.g., Kahl et al., 2011; Patanè et al., 2013). Many volcanic eruptions are thought to be initiated by intrusion of hot, primitive magma into an existing reservoir within the volcanic plumbing system (e.g., Sparks et al., 1977; Aiuppa et al., 2017). The timing and storage duration of these intrusions are usually poorly known, especially for pre-historic eruptions. Geophysical evidence of such a magma mixing event may be absent or give ambiguous results.

For example, magma mixing may occur aseismically (e.g., Klein et al., 1987; Johnson, 1992) and increases in tilt that are normally attributed to magma influx may be related to excess gas rather than the arrival of magma to a shallow reservoir system (e.g., Johnson, 1992; Aiuppa et al., 2017). Consequently, developing new tools that document short-lived events is crucial to understanding the timing of the magmatic processes that precede and possibly trigger volcanic eruptions.

Olivine is a common phenocryst in basaltic magmas. Studying its chemical zoning patterns has proven invaluable for gaining a better understanding of the timescales of magmatic processes operating in diverse tectonic settings (e.g., Costa and Dungan, 2005; Ruprecht and Plank, 2013; Shea et al., 2015a; Bouvet de Maisonneuve et al., 2016; Lynn et al., 2017). For example, timescales of weeks to years that broadly correspond to periods of volcanic unrest (e.g., Kahl et al., 2011; Albert et al., 2015) are now routinely determined by modeling diffusion-controlled concentration gradients of major and minor elements in olivine (Fe–Mg, Ni, Mn, Ca; Fig. 1). These elements are typically used to characterize pre-eruptive magmatic processes that operate over weeks to centuries in mafic volcanic systems (Fig. 1). Longer timescales (years to

* Corresponding author at: Department of Geological Sciences, University of Delaware, Newark, DE 19716, USA.

E-mail address: kjlynn@udel.edu (K.J. Lynn).

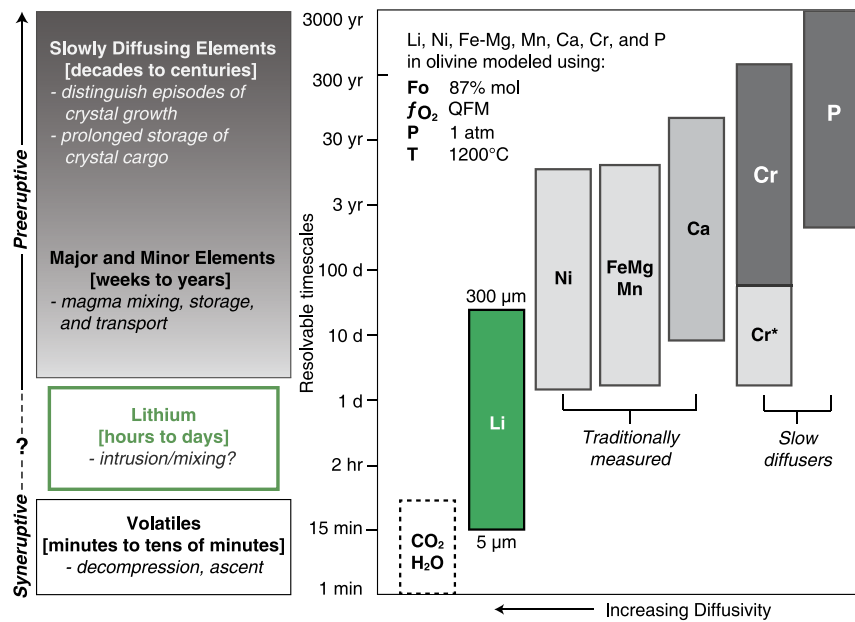


Fig. 1. Lithium is a rapidly diffusing trace element in olivine (green box; vacancy mechanism of ${}^7\text{Li}$ from Dohmen et al., 2010) that provides a unique view into the pre-eruptive processes operating on timescales of a few hours to a few days. Timescales of syneruptive processes operating over as little as a few minutes have recently been proposed using CO_2 and H_2O diffusion through phenocryst-hosted melt embayments (dashed box; Lloyd et al., 2014; Ferguson et al., 2016). Pre-eruptive magmatic processes such as magma mixing, storage, and transport are characterized using the diffusion of traditionally measured major (Fe–Mg, light grey box; Dohmen and Chakraborty, 2007a, 2007b) and minor elements (Ni, Mn, Ca, Cr^* , light grey boxes; Petry et al., 2004; Coogan et al., 2005; Holzapel et al., 2007; Cr^* is a faster D_{Cr} value from Jollands et al., 2018). The oldest histories of crystal growth and/or prolonged storage are usually inferred from slowly diffusing trace elements, such as Cr and P (dark grey boxes; Ito and Ganguly, 2006; Watson et al., 2015). (For interpretation of the colors in the figure(s), the reader is referred to the web version of this article.)

decades) representing episodes of crystal growth and storage can be inferred from trace elements, typically Cr and P, that are more slowly modified by diffusion (e.g., Bouvet de Maisonneuve et al., 2016; Fig. 1).

Timescales of minutes to tens of minutes correspond to syneruptive processes such as degassing and magma ascent (Fig. 1). The decompression and rapid diffusion of CO_2 and H_2O in glasses from mineral-hosted melt embayments (Lloyd et al., 2014; Ferguson et al., 2016) and the diffusive loss of hydrogen from olivine (e.g., Demouchy et al., 2006) have been modeled to access short timescales of syneruptive processes. However, embayments are rare and measuring and interpreting hydrogen concentrations in olivine is challenging, resulting in large analytical uncertainties. Thus, there remains a critical pre-eruptive period of hours to days that is largely inaccessible using traditional geospeedometers. Characterizing the magmatic processes operating in this enigmatic window of time remains a fundamental challenge for modern petrology and volcanology.

1.2. Lithium chronometry

Lithium is a rapidly diffusing trace element in olivine that can provide a unique perspective on magmatic processes that occur over hours to days in basaltic magma (Fig. 1; Dohmen et al., 2010). Lithium is moderately incompatible (e.g., $K_{\text{Li}}^{\text{ol/melt}} = 0.1\text{--}0.2$; Grant and Wood, 2010), and its partitioning behavior apparently does not strongly depend on pressure, temperature and mineral composition (Seitz and Woodland, 2000). The rapid diffusion of Li (Fig. 1) results in the complete re-equilibration of olivine crystals <1 mm in diameter after only a few months at temperatures near 1200°C (Tomascak et al., 2016). Thus, Li zoning is expected to be unrelated to the longer-term magma mixing history preserved by Fe–Mg, Ni, and Mn (Fig. 1), and potentially records additional information about short-lived processes. Lithium diffusion in olivine can occur via two mechanisms: a vacancy-controlled, ‘slower’ mode, and an interstitial ‘faster’ mode (Dohmen et al., 2010). Signif-

icant mass-dependent diffusive fractionation of ${}^6\text{Li}$ and ${}^7\text{Li}$ can occur in olivine with high Li contents (e.g., 10s or 100s of ppm in doped experiments and natural samples; Dohmen et al., 2010; Weyer and Seitz, 2012; Richter et al., 2017). However, at concentrations of only a few ppm and high temperatures typical of basaltic systems (e.g., near 1200°C), it is thought that the diffusion of Li concentrations may be modeled using the slower vacancy mechanism of ${}^7\text{Li}$ (Dohmen et al., 2010).

In this study, lithium concentrations in volcanic olivine are modeled in basalts from Kīlauea Volcano. Rapidly quenched tephra from the recent prehistoric (1500 to ~ 1820 CE) Keanakāko’i Tephra (KT) explosive eruptions were chosen for this study because little is known about the physical or chemical controls on the eruption dynamics during this time, and Li diffusion can help to identify processes occurring shortly before and potentially during these eruptions. The basaltic pumice in these deposits are ideal for Li diffusion because they contain fresh, glass-coated olivine produced during a period of exceptionally low magma supply ($\sim 2\%$ of average output during the historical period after 1823; Swanson et al., 2014). These glass and olivine are among the most primitive sub-aerial deposits at Kīlauea (glass MgO up to 11.2 wt.% and forsterite values of 89%; Lynn et al., 2017; Garcia et al., 2018). The heterogeneous glasses (e.g., 6.5–11.0 wt.% MgO) in several KT units were interpreted to reflect inefficient mixing and little or no storage of the high-MgO magma in the reservoir system (Helz et al., 2015; Garcia et al., 2018). Thus, these more primitive eruption products may not have been stored for years to decades in a shallow magma chamber like Kīlauea’s historical lavas (Garcia et al., 2003; Pietruszka et al., 2015).

Basaltic deposits from six eruptions, three from phreatomagmatic and three from high lava-fountaining eruptions within the Keanakāko’i Tephra are utilized because their rapid quenching (seconds to minutes) preserves information relevant to magmatic processes by avoiding the longer cooling histories (hours to days) following eruption that are typical of effusive lava flows (e.g., Hon et al., 1994). These samples are ideal for applying the lithium

geospeedometer since olivine crystals are euhedral, allowing them to be crystallographically oriented and sectioned through their cores and their longer-term magmatic histories (weeks to years) were previously characterized by modeling forsterite (Fo; $[\text{Mg}/(\text{Mg} + \text{Fe}) \times 100]$) and Ni zoning (Lynn et al., 2017). Thus, KT olivine crystals provide an exceptional opportunity to establish constraints on late-stage, short duration magmatic events that may prime basaltic systems for volcanic eruptions.

2. Samples and methods

2.1. Sample selection and preparation

The Fo and Ni contents, zoning patterns, and associated time-scales of the KT olivine crystals used in this study are well documented (Lynn et al., 2017). These samples are renamed here following the new stratigraphic nomenclature proposed for the Keanakāko'i Tephra (Swanson and Houghton, 2018). Olivine crystals were selected from three informal phreatomagmatic beds, two within Unit D (D_1 and D_2, previously referred to as u7 and u11 by Lynn et al., 2017, respectively) and one within Unit F (previously u20). Three additional samples include the juvenile tephra Units B, K1, and K2 (previously the Basal Reticulite, Golden Pumice, and Eastern Pumice, respectively; see Swanson et al., 2012 and Swanson and Houghton, 2018 for detailed unit descriptions). KT olivine crystals were oriented perpendicular to the *a*- or *b*-axes (with the *c*-axis in the plane of the section) and carefully ground and polished to their core. This careful sample preparation aided in minimizing 3D effects on diffusion timescales derived from 1D modeling and avoids off-center and oblique sections that can introduce significant error (up to 25×) in diffusion timescale estimates (Shea et al., 2015b).

2.2. Laser ablation inductively coupled plasma mass spectrometry (LA-ICPMS)

Trace element analyses were acquired at the Earth Observatory of Singapore (Nanyang Technological University) using a Photon Machines Analyte G2 excimer laser connected to an iCAP Q ICPMS in an Ar–He atmosphere. Machine settings were optimized to reduce oxide production and interferences by achieving a ThO^+ signal intensity of <0.6% of the Th^+ signal. The laser was run at 70% output and 8 Hz with constant voltage and 240 shot count. For all analyses, 20 s of background signal (laser off) were acquired followed by 40 s of ablation signal (laser on). To achieve high precision measurements of Li only seven elements were analyzed. This allowed significantly longer dwell times on ^7Li than typical multi-element (e.g., 20+) analytical routines allow.

Data reduction in Lolite© (Paton et al., 2011) removed the first and last three seconds of counts for each analysis before converting counts to concentrations. The isotope ^7Li was measured for 25 transects in 22 olivine crystals using $10 \times 50 \mu\text{m}$ spots oriented with the long length parallel to the crystal–melt boundary (Supplementary Material, Fig. S1). An $11 \mu\text{m}$ spacing was used to avoid overlap and to create a $1 \mu\text{m}$ separation between individual spot analyses. The internal reference isotope ^{29}Si was used to convert raw counts to concentrations based on the EPMA measurements of SiO_2 in olivine (taken from Lynn et al., 2017). The NIST 612 silicate glass was used to calibrate relative sensitivities (40.2 ppm Li), and NIST 610 and USGS BCR-2G were run as unknowns (468 and 9 ppm, respectively; see Supplementary Data File). The three reference materials were analyzed in between each olivine transect to monitor instrumental drift. Analytical precision (2σ) for repeated measurements of NIST 612 glass is ± 0.8 ppm for Li (2% relative to preferred GeoReM value of 40.2 ppm; Supplementary Data File). Average values for the other reference materials are

468 ppm (± 4 ppm or 0.8%) for NIST 610 and 8.4 ppm (± 0.24 ppm or 2.6%) for BCR-2G (see Supplementary Data File). These values were compared to the GeoReM database preferred values (Jochum et al., 2011, 2016) to assess data quality. Average 2σ SD errors for Li measurements of KT olivine crystals were ± 0.08 ppm and were calculated by Lolite© (Paton et al., 2011). Our reported errors are much lower than typical LA-ICPMS analyses of Li (cf. de Hoog et al., 2010 with ± 0.07 ppm at 1σ) due to the reduced number of elements (seven) analyzed in our routine.

2.3. Diffusion modeling

Smoothed lithium concentration gradients were modeled using finite differences and the one-dimensional form of Fick's Second Law:

$$\frac{\partial C}{\partial t} = D \frac{\partial^2 C}{\partial x^2} \quad (1)$$

where C is concentration, t is time, D is the diffusion coefficient, and x is distance (Crank, 1975). The diffusivity of Li ($D_{7\text{Li}}$) parallel to the *c*-axis can be calculated using the Arrhenius relation (Dohmen et al., 2010):

$$\log(D_{7\text{Li}}) = -5.92(\pm 1.0) - 1.2847 \times \frac{10^4}{T(\text{K})} \quad (2)$$

where T is the temperature in Kelvin. This expression is appropriate for diffusion in olivine containing 1–10 ppm Li and temperatures between 800 and 1200 °C (Dohmen et al., 2010). Model temperatures were assumed to be constant and were obtained using the Kilauea glass–MgO thermometer (uncertainty of ± 10 °C; Helz and Thornber, 1987) and the inferred melt Mg# in equilibrium with olivine rim Fo contents ($K_{\text{Fe-Mg}}^{\text{ol/melt}} = 0.343 \pm 0.018$; Matzen et al., 2011) following the methods described in Lynn et al. (2017). These temperatures ranged from 1245 to 1275 °C (Table 1) and are akin to the magma temperature for mixing and diffusion recorded by each crystal. Lithium concentration gradients were modeled using Equations (1) and (2) to retrieve timescales corresponding to the last thermal and/or chemical perturbation experienced by the host magma. Initial boundary conditions were determined based on the compositions of olivine cores (C_0 , the Li content of the crystal before thermodynamic perturbation) and crystal rims (C_1), which are inferred to reflect diffusion with the host melt after perturbation. The minimum resolvable timescale (accurate to within 20% of the actual timescale) for a spatial resolution of $11 \mu\text{m}$ is 4.5 h (Bradshaw and Kent, 2017) at a representative model temperature of 1250 °C and the vacancy mechanism of Li diffusion (Dohmen et al., 2010). No Li diffusion anisotropy between different crystallographic axes were resolved within the spatial limitations of the method (e.g., $11 \mu\text{m}$ spacing) for three crystals analyzed for which two perpendicular traverses were measured (comparing the *b*- to *c*-axis, and *a*- to *b*-axis).

3. Results

Lithium concentration profiles in KT olivine are characterized by a gradual decrease ($\text{Li}_{\text{core}} > \text{Li}_{\text{rim}}$, normal zoning; Fig. 2a, 2c) or increase ($\text{Li}_{\text{core}} < \text{Li}_{\text{rim}}$, reverse zoning; Fig. 2b, 2d) of 0.2–1.6 ppm Li across a smooth gradient 20–400 μm long. Olivine crystals are typically ~ 1 mm in diameter and all profiles in this study have clearly preserved concentration plateaus, indicating that core Li contents are probably unaffected by diffusive re-equilibration. Lithium zoning is inversely correlated with Fo, but Li profiles have different diffusion distances into the olivine compared to Fo (Fig. 2; see also Supplementary Material, Fig. S2). Lithium concentrations were normalized and examined on a log scale for inflection features or

Table 1
Calculated times (days) obtained by modeling the chemical diffusion of Li in olivine crystals.

Unit ^a	Ol. ^b	Core Fo	T (°C)	Li C ₀	Li C ₁	Zoning type	t _{Li} (days) ^c	Δ (–)	Δ (+)
B	28	78.8	1245	5.20	2.50	N	8	7	17
	10	86.9	1245	1.41	1.71	R	8	6	12
	12	87.4	1263	1.50	1.25	N	2	1.5	4
D_1	20	87.3	1245	1.42	1.57	R	2	1	3
	12_1	88.4	1245	1.35	1.75	R	1.5	0.5	0.5
	12_2	88.4	1245	1.35	1.69	R	0.6	0.4	0.4
	28_1	89.4	1245	1.35	1.45	R	2.5	2	7.5
	28_1	89.4	1245	1.32	1.45	R	1.5	0.25	4.5
D_2	6	88.5	1275	1.50	1.10	N	1	0.75	6
	1	88.7	1275	1.30	1.59	R	3	2.75	9
F	21	77.0	1263	1.90	2.80	R	22	10	18
	27	79.2	1263	3.40	1.75	N	18	4	5
	23	82.6	1263	2.40	1.67	N	6	4	6
	35_1	83.9	1263	1.90	1.60	N	9	5	11
	35_2	83.9	1263	2.00	1.60	N	3	1	17
	18	86.4	1263	1.85	1.57	N	2.5	1.75	4.5
	7	87.6	1263	1.80	1.36	N	10	2	–
	29	88.4	1263	1.52	1.61	R	2	1.5	6
	K1	32	88.2	1237	1.50	2.20	R	14	6
34		88.3	1237	1.40	2.15	R	10	5	14
4		88.7	1237	1.37	1.50	R	2	1.9	6
K2	15	85.1	1237	1.63	1.50	N	20	15	50
	18	85.6	1237	2.10	1.60	N	2.5	1.75	4.5
	3	87.5	1237	1.55	2.05	R	4	3.5	6
	19	88.1	1237	1.40	2.00	R	1.5	0.75	2.5

^a Revised sample names following Swanson and Houghton (2018).

^b Olivine sample number, and profile number within the olivine where appropriate (e.g., 10_1 and 10_2). Fo (forsterite; [100 × Mg/(Mg + Fe)]) contents and temperatures are from Lynn et al. (2017).

^c Timescales retrieved using D_{7Li} from Dohmen et al. (2010). If the faster D_{6Li} is used the primary distribution of timescales would be on the order of seconds to minutes. Lithium zoning types are either N (normal) or R (reverse). Initial boundary conditions for the core (C₀) and rim (C₁; nomenclature after Costa and Dungan, 2005) used in diffusion models are reported in ppm. All reported timescales are best-fit results within analytical uncertainty and noise. (–) and (+) represent the errors calculated by finding the minimum and maximum fits by visual inspection of the scatter in the data (see examples in Fig. 2). A dash under (+) denotes a profile in which scatter outliers make it difficult to determine the maximum timescale error.

changes in concavity that might indicate isotopic fractionation of ⁶Li and ⁷Li (Richter et al., 2017). No such features were found for KT samples (see Supplementary Material, Fig. S2). Furthermore, the expected fractionation of ⁶Li from ⁷Li during sub-ppm Li diffusion (typical of basaltic systems) is reported to be <5‰ (Parkinson et al., 2007) and would be difficult to resolve with secondary ion mass spectrometry. Li concentration gradients of a few ppm in KT olivine may thus be modeled by the vacancy mechanism of ⁷Li diffusion, consistent with the high temperatures (>1200 °C) and low Li abundance (<5 ppm) in these samples (Dohmen et al., 2010).

Lithium timescales for all KT eruptions range from less than one day to three weeks (Table 1). The calculated timescales are subject to relatively large errors (average is –60% and +220% relative to best fit value; Table 1) due to the 2σ analytical error and spacing of the analysis (1 spot per 11 μm; for example, see Fig. 2). Therefore, all timescales are presented with minimum, maximum, and best fit results based on visual inspection of individual profiles (e.g., 1.5 ± 0.5 days; Table 1) to provide robust estimates of potential re-equilibration timescales. Timescale uncertainties related to temperature calculations (±10 °C; Helz and Thornber, 1987) are on average 10% of the timescale calculated for a given profile (e.g., if the best-fit is 18 days, uncertainty related to temperature is approximately ±2 days), which we note is smaller than the range provided by minimum and maximum determinations from consideration of 2σ error.

Most Li timescales (60%) are less than four days (Fig. 3a). This is much shorter than the typical weeks to years retrieved from modeling with traditional geospeedometers (Fig. 3b). The shortest Fo and longest Li timescales rarely overlap in individual eruptions (Supplementary Material, Fig. S3). There is generally no correlation

between Li timescale and olivine Fo content, with the exception of the <Fo₈₀ crystals in Unit F (Table 1). There are also no systematic correlations between Li timescale duration and zoning type (normal vs. reverse), eruptive style (phreatomagmatic or high lava fountain), or stratigraphic order of the eruptive units (Table 1; see also Supplementary Material, Fig. S4).

4. Discussion

4.1. Element coupling

Possible charge-balancing behavior of Li with other minor or trace elements in minerals can complicate the interpretation that concentration gradients are solely driven by diffusion (Cooper et al., 2017; Rubin et al., 2017; Tang et al., 2017; Wilson et al., 2017). Some Keanakāko'i Tephra olivine show clear correlations between Li and P zoning within laser ablation profiles (Supplementary Material, Fig. S5) that will be the subject of a separate contribution examining Li, Al, P, and Cr coupling in olivine. To avoid potential element coupling complications, only profiles that showed no systematic correlations between Li and any minor (Ca, Ni, Mn) or trace elements (P, Al, Cr, Na) were modeled. Obvious differences in the diffusion distances of Li and Fe–Mg (Fo) zoning within single olivine crystals also show that Li diffusion is not coupled to major elements (Supplementary Material, Fig. S6).

4.2. Distinguishing magmatic processes recorded in Li concentrations in glass and olivine

The interpretation of Li concentrations in basaltic melt and olivine can be more complex than many other trace elements.

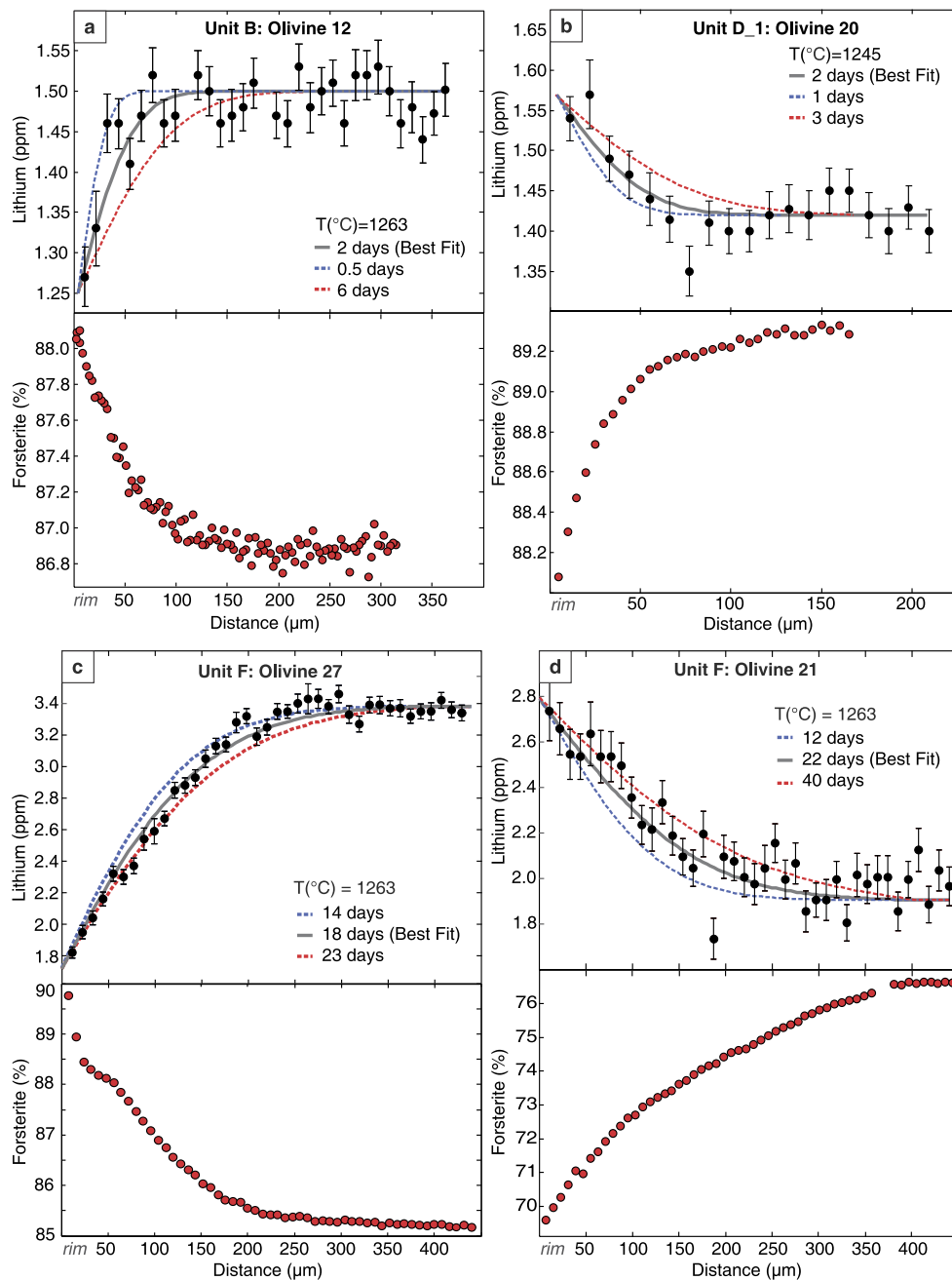


Fig. 2. Rim-to-core lithium zoning examples for olivine phenocrysts that span a range of Li timescales and Fo zoning types. **a.** Normally zoned Li (ppm) and reversely zoned Fo (%) profiles for Unit B olivine 12 (Table 1). **b.** Reversely zoned Li and normally zoned Fo for Unit F olivine 19. **c.** Normally zoned Li and reversely zoned Fo for Unit F olivine 27. **d.** Reversely zoned Li and normally zoned Fo for Unit K2 olivine 19, the lowest Fo olivine in the study. All LA-ICPMS data are presented with 2σ error bars for individual spot analyses (generally ± 0.08 ppm). Modeled timescales for all crystals have minimum (dashed blue line), best fit (solid grey line), and maximum (dashed red line) values. Temperatures were obtained using the Kilauea glass MgO thermometer (Helz and Thornber, 1987) and the inferred melt Mg# in equilibrium with the general population of olivine rim Fo contents ($Kd_{\text{Fe-Mg}}^{\text{ol/melt}} = 0.343 \pm 0.018$; Matzen et al., 2011) following the methods described in Lynn et al. (2017).

Mantle source heterogeneity and fractional crystallization dominate the concentration of incompatible trace elements like Nb and Y in KT glasses and melt inclusions (e.g., Sides et al., 2014; Garcia et al., 2018). Lithium is moderately incompatible in olivine (e.g., 0.1–0.2; Grant and Wood, 2010), and apparently weakly volatile ($Kd_{\text{Li}}^{\text{vapor/melt}} \sim 0.1$; Edmonds, 2015) in Kilauea magmas. The Li concentration in the melt should therefore increase during fractional crystallization of olivine, but to a lesser extent if degassing is involved. A simple fractionation and degassing model (e.g., Vlastelic et al., 2011) predicts that fractional crystallization is expected to play the dominant role in generating melt Li variabil-

ity using the above value (Fig. 4). Only when $Kd_{\text{Li}}^{\text{vapor/melt}}$ is large (e.g., 10; Fig. 4) does degassing make a significant difference in Li melt content (Supplementary Material, Fig. S7). Comparison of this model with Rb vs. Li glass data from KT eruptions ($R^2 = 0.8$; Sides et al., 2014) shows that fractional crystallization is sufficient to explain most of the range in melt Li concentrations. Variable Rb contents at a given MgO within a single eruption (e.g., Unit K1, Fig. 4) also show that mantle source variability likely generates second-order scatter in incompatible trace elements, such as Li and Rb.

Both normal and reverse lithium zoning patterns are found in olivine crystals from individual KT eruptions (Fig. 2). These re-

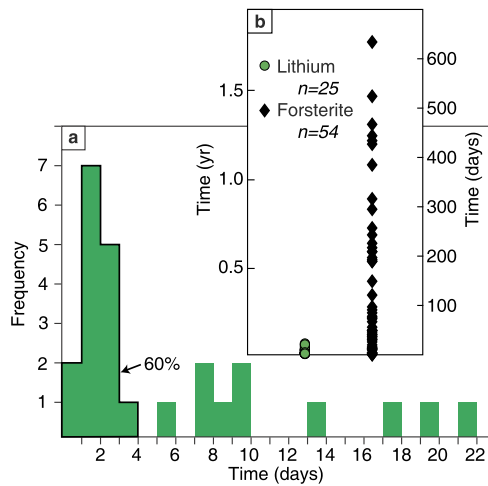


Fig. 3. Frequency and distribution of timescales retrieved from modeling the diffusive re-equilibration of multiple elements in KT olivine. **a**, Timescales retrieved from lithium zoning. Bins represent 1 day, where 60% of all timescales are ≤ 4 days. **b**, Lithium and Fo timescales (Lynn et al., 2017) for the same KT eruptions.

sults demonstrate that the zoning was not produced by fractional crystallization alone. This has not been documented in other studies of Li zoning in magmatic olivine (e.g., Parkinson et al., 2007; Weyer and Seitz, 2012). The general increase in Li content with fractional crystallization supports the interpretation that Li diffusion profiles were generated by mixing of a low-Li primitive component and a higher-Li evolved melt component. This interpretation is consistent with previous studies that invoked mixing of KT endmembers (recharge and reservoir) to explain a wide range of glass MgO contents (Helz et al., 2015; Garcia et al., 2018) and olivine populations (Lynn et al., 2017). These mixing events likely included melts that evolved past olivine control (e.g., <7.2 wt.% MgO; Wright and Fiske, 1971), which are common in some Keanakāko'i Tephra units (Helz et al., 2015; Lynn et al., 2017; Garcia et al., 2018). Primitive intrusions mixed with an array of stored melt compositions throughout the KT period, each the end-result of fractional crystallization (\pm previous magma mixing, source variability, and possibly degassing), probably contributed to the diversity of Li zoning found in KT olivine. The variations of Li concentrations are likely related mainly to fractional crystallization and subsequent diffusive re-equilibration as a result of magma mixing. We therefore interpret the lithium zoning patterns to record the timing of mixing between hot, primitive magma and more evolved, stored magma(s) shortly before eruption.

4.3. The tempo of eruption initiation

The days to weeks timescales from lithium chronometry, combined with our previous timescales of weeks to years from Fo and Ni zoning (Lynn et al., 2017), provide a new and more comprehensive magmatic history for Kīlauea's recent 300-yr period of explosive activity. Zoning of Fe–Mg and Ni in KT olivine shows that most mantle-derived recharge magmas were mixed and then stored for weeks to years in crustal reservoirs beneath the summit (Lynn et al., 2017; Fig. 5a). This longer-term storage history is not preserved by Li because its faster diffusion results in the complete re-equilibration of Li in olivine crystals of the typical size observed in KT samples (~ 1 mm in diameter) after as little as a few months at temperatures near 1200 °C (Tomascak et al., 2016). Thus, the observed Li zoning in KT olivine documents some additional mixing event hours to days prior to eruption (Fig. 5b). The history of mixing recorded by Fe–Mg, Ni, and now also Li support the argument that most KT magmas had complex pre-eruptive his-

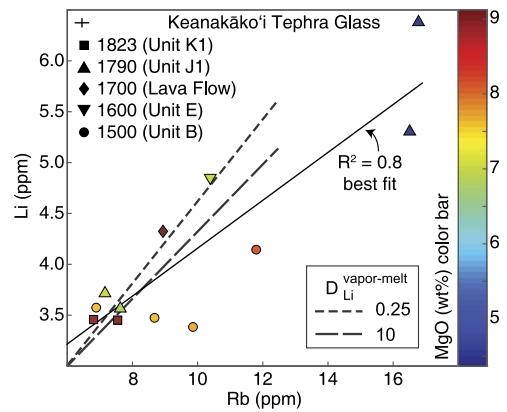


Fig. 4. Matrix glass Rb (ppm) vs. Li (ppm) contents with color scale indicating MgO (wt.%) for Keanakāko'i Tephra glasses from Sides et al. (2014). The correlation between Li and Rb indicates that fractional crystallization played a strong role in generating melt Li variability. Magma mixing between low-Li primitive and higher-Li evolved melts (from fractional crystallization) then creates the zoning observed in KT olivine.

tories that preclude simple, rapid ascent from mantle depths to the surface as was advocated by Sides et al. (2014).

Lithium zoning is interpreted here to record the intrusion of a recharge magma into a relatively evolved reservoir typically a few days prior to eruption (Fig. 5b). Mixing likely occurred within Kīlauea's summit reservoir system at depths of 1.5–5.0 km (Poland et al., 2014), perhaps near 1.5–2.0 km deep as suggested by volatile diffusion in three melt embayments within KT olivine crystals (Ferguson et al., 2016). First-order magma ascent rates can be estimated using these depths and the primary distribution of lithium timescales in this study (6 h–4 days; Table 1 and Fig. 3). The maximum ascent rates for timescales of 6 h are ~ 0.1 m/s from a depth of 2 km and 0.23 m/s if magmas lower in the reservoir system ascended from 5 km depth. Ascent rates from the embayment study are much faster: 3–17 m/s calculated from ascent timescales of 2–7 min. However, there are only three total embayments from two different KT eruptions. The timescales in this limited dataset represent $<2\%$ of the total time recorded by Li diffusion, demonstrating that volatile diffusion likely records syneruptive processes during ascent, whereas Li diffusion records the timing of a pre-eruptive mixing event (Fig. 5b).

4.4. Hazard implications of a short window between intrusion and eruption

Identifying late-stage mixing events with Li diffusion in olivine provides critical insights into understanding precursor geophysical or geodetic signals that may warn of imminent eruptions. The short duration recorded by Li zoning suggests that the time between intrusion and eruption was short, providing only hours to days of warning before a potentially hazardous eruption. However, many KT eruptions have olivine crystals that record Li timescales of hours to several days and also Fe–Mg and Ni timescales of weeks to years (Lynn et al., 2017). These results suggest that some intrusions may not have led to eruption (cf., many Kīlauea intrusions between 1963–1983; Klein et al., 1987). These data and field evidence suggest that magma intrusion and eruption during the KT period was episodic. This behavior contrasts strongly with Kīlauea's past 60 yrs of historical activity, in which orders of magnitude higher magma flux resulted in essentially continuous supply to the shallow reservoir system (Swanson et al., 2014; Poland et al., 2014; Pietruszka et al., 2015). Thus, Li zoning suggests that the frequency and timing of magma delivery in a future explosive eruptive period may have different signals of unrest prior to eruption (consistent with previous interpretations by Swanson et al., 2014), punctu-

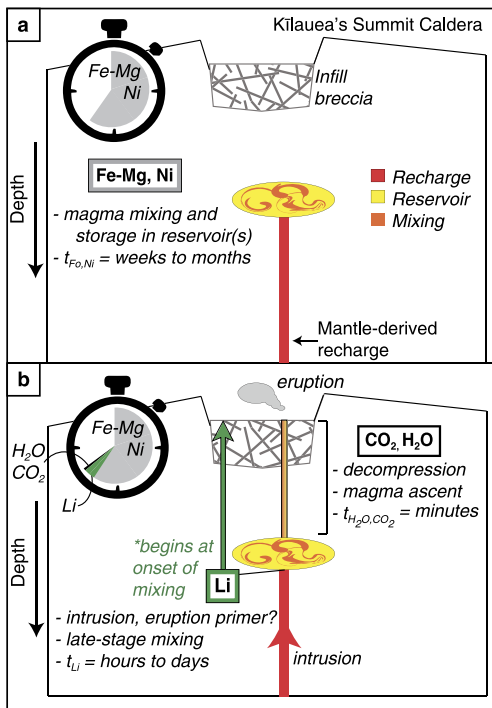


Fig. 5. Simplified schematic of Kilauea's shallow reservoir system illustrating the magmatic processes recorded by chemical zoning. **a.** Major and minor elements record early mixing and storage events ($t_{Fe,Ni}$). Mantle-derived recharge magmas (red) intersect stored reservoir magma (yellow), producing hybrid compositions (orange). The storage time after mixing (weeks to years; grey on stopwatch) is recorded by Fe–Mg and Ni zoning (Lynn et al., 2017). **b.** A new intrusion of mantle-derived magma enters the shallow plumbing system (t_{Li}). The remobilization of the stored magma and degassing of the relatively volatile-rich intrusion occurs over hours to days (green on stopwatch). Syneruptive diffusion of volatiles from phenocryst-hosted melt embayments (t_{H_2O,CO_2}) record magma decompression and ascent over timescales of a few minutes (black on stopwatch; Ferguson et al., 2016).

ated by discrete recharge events into the shallow plumbing system.

4.5. Multiple pulses of magma mixing at basaltic volcanoes

Intrusion of mafic magma is commonly invoked as the trigger for volcanic eruptions (e.g., Sparks et al., 1977; Aiuppa et al., 2017), although the timing and number of these events is usually poorly known. Petrologic evidence of magma mixing such as complex chemical and textural zoning is common when the end-member mixing components have significant geochemical and rheological differences (e.g., 1915 eruption at Lassen Volcano; Clyne, 1999). Magma mixing between more compositionally similar melts at Kilauea or Mt. Etna (Sicily) is generally less obvious and best preserved in mineral zoning patterns (e.g., Kahl et al., 2011). With the addition of the Li chronometer, diffusion in olivine can now be used to recognize multiple basaltic mixing events that might have occurred up to a few hours prior to eruption. During the KT period at Kilauea, the final mixing event that primed the system for eruption was identified by Li zoning and probably occurred within a few days of magma ascent to the surface (Fig. 3). These datasets provide an important framework for the interpretation of seismic, geodetic, and gas monitoring data that might represent the onset of future explosive eruptive periods.

Diffusion timescales related to the most recent mixing event prior to eruption may also provide insights on crustal magma ascent rates. Nickel zoning in olivine crystals from Irazú Volcano (Costa Rica) record magma ascent from the mantle (30–35 km) in 4–7 months, with ascent rates estimated at 55–80 m/day (Ruprecht and Plank, 2013). This approach cannot be used to extract as-

cent rates from KT olivine because the Ni zoning patterns were determined to record weeks to years of storage after mixing in shallow crustal chambers (Lynn et al., 2017). Diffusion of Fe–Mg in olivine has also been linked to historical accounts of seismicity leading up to mafic monogenetic eruptions in Tenerife (Canary Islands; Albert et al., 2015). The combined datasets were used to infer magma ascent after an intrusion into some shallow storage reservoir two weeks prior to the eruptions. The mobilization of magma from intrusion to eruption during the KT period at Kilauea must have occurred too quickly to be recorded by Fe–Mg diffusion (Fig. 3b), and there are no historical accounts of KT eruptions with which to compare petrologic timescales. Thus, information gained from Li zoning is an integral part of understanding basaltic eruption dynamics at Kilauea and potentially other basaltic volcanoes.

Lithium can also be used to explore whether intrusions occurring just prior to eruption are recorded in olivine from other basaltic systems. In March 1998, a seismic swarm at Piton de La Fournaise (Réunion) indicated the arrival of new magma into the shallow reservoir system that migrated from a depth of 7.5 km to the surface within three days (Battaglia et al., 2005). The three days between intrusion and eruption as indicated by the seismic swarm is at the limit of timescale resolution using intermediate diffusing species like Fe–Mg and Ni (Fig. 1). Lithium zoning in rapidly quenched olivine (e.g., from tephra) could instead be used to independently test if the intrusion mixed with resident magma before ascending to the surface. In this way, extracting information about late stage mixing from Li zoning at Piton de La Fournaise, Mt. Etna, and other frequently active basaltic volcanoes will aid in understanding what primes and ultimately drives eruptions. These data will also expand our understanding of crustal ascent rates, where Li chronometry could be a robust petrological compliment to magma storage and transit recorded by seismicity.

5. Conclusions

Understanding the short-duration magmatic processes leading up to volcanic eruptions is essential for constraining future eruption scenarios yet remains difficult to characterize using established petrologic and geophysical methods. We have shown that zoning of lithium concentrations in olivine can be used to identify the processes that potentially trigger basaltic eruptions. At Kilauea Volcano olivine zoning records petrologic evidence of late-stage magma mixing events for prehistoric explosive eruptions of the Keanakāko'i Tephra. Olivine crystals yield Li diffusion timescales that are typically <4 days, which reflects the intrusion of higher-MgO, mantle-derived magma that probably primed the shallow plumbing system for eruption. These data are critical for assessing potential hazards and preparing for future episodes of dominantly explosive activity that at Kilauea can last for several centuries (Swanson et al., 2014). Timescales from Li diffusion in basaltic eruptions may generally be much shorter than those from Fe–Mg and Ni zoning and can reveal late-stage intrusions that might have otherwise been overlooked if only traditional geospeedometers were applied. Thus, Li diffusion used in tandem with other geospeedometers (e.g., Fe–Mg, Ni, CO₂, H₂O) should be used to characterize the magmatic processes that trigger eruptions at basaltic volcanoes. Investigating late-stage magmatic histories provides key data for understanding the physical and chemical controls on eruption initiation and crustal magma ascent rates. This approach is invaluable for understanding prehistoric eruptions, which might yield critical insights into the warning signs of future eruptive episodes so that basaltic eruption scenarios can be better constrained.

Acknowledgements

The authors thank Gareth Fabbro for assistance with LA-ICPMS analyses, Eric Hellebrand for help with EPMA, Don Swanson for sample collection, and Eileen Chen for sample preparation. We are grateful to Adam Kent and E. Bruce Watson for constructive reviews and Tamsin Mather for editorial handling. This work was supported by the Fred M. Bullard Graduate Fellowship (University of Hawai'i) and a National Science Foundation (NSF) East Asia and Pacific Summer Institutes grant (OISE15-13668) to K.J.L. Additional support was provided by NSF grants to M.G. (EAR13-47915 and EAR14-49744) and T.S. (EAR13-21890), and a National Research Foundation Singapore Investigatorship Award (NRF-NRFI2017-06) to F.C. This is SOEST contribution number 10431.

Appendix A. Supplementary material

Supplementary material related to this article can be found online at <https://doi.org/10.1016/j.epsl.2018.08.002>.

References

- Aiuppa, A., Bitetto, M., Francofonte, V., Velasquez, G., Parra, C.B., Guidice, G., Liuzzo, M., Moretti, R., Mussallam, Y., Peters, N., Tamburello, G., Valderrama, O.A., Curtis, A., 2017. A CO₂-gas precursor to the March 2015 Villarrica volcano eruption. *Geochem. Geophys. Geosyst.* 18. <https://doi.org/10.1002/2017GC006892>.
- Albert, H., Costa, F., Martí, J., 2015. Timing of magmatic processes and unrest associated with mafic historical monogenetic eruptions in Tenerife Island. *J. Petrol.* 56 (10), 1945–1966. <https://doi.org/10.1093/ptrology/egv058>.
- Battaglia, J., Ferrazzini, V., Staudacher, T., Aki, K., Cheminée, J.-L., 2005. Pre-eruptive migration of earthquakes at the Piton de La Fournaise volcano (Réunion Island). *Geophys. J. Int.* 161 (2), 549–558. <https://doi.org/10.1111/j.1365-246X.2005.02606.x>.
- Bouvet de Maisonneuve, C., Costa, F., Huber, C., Vonlanthen, P., Bachmann, O., Dungan, M.A., 2016. How do olivines record magmatic events? Insights from major and trace element zoning. *Contrib. Mineral. Petrol.* 171, 56. <https://doi.org/10.1007/s00410-016-1264-6>.
- Bradshaw, R.W., Kent, A.J.R., 2017. The analytical limits of modeling short diffusion timescales. *Chem. Geol.* 466, 667–677. <https://doi.org/10.1016/j.chemgeo.2017.07.018>.
- Clyne, M.A., 1999. A complex magma mixing origin for rocks erupted in 1915, Lassen Peak, California. *J. Petrol.* 40 (1), 105–132. <https://doi.org/10.1093/ptrology/40.1.105>.
- Coogan, L.A., Hain, A., Stahl, S., Chakraborty, S., 2005. Experimental determination of the diffusion coefficient for calcium in olivine between 900 °C and 1500 °C. *Geochim. Cosmochim. Acta* 69 (14), 3683–3694. <https://doi.org/10.1016/j.gca.2005.03.002>.
- Cooper, K.M., Till, C.B., Kent, A.J.R., Costa, F., Rubin, A.E., Gravley, D., Deering, C., Cole, J., Bose, M., 2017. Response to comment on “Rapid cooling and cold storage in a silicic magma reservoir recorded in individual crystals”. *Science* 358, eaap9145. <https://doi.org/10.1126/science.aap9145>.
- Costa, F., Dungan, M., 2005. Short time scales of magmatic assimilation from diffusion modeling of multiple elements in olivine. *Geology* 33 (10), 837–840.
- Crank, J., 1975. *The Mathematics of Diffusion*, 2nd ed. Oxford Science Publications, Oxford.
- de Hoog, J.C.M., Gall, L., Cornell, D.H., 2010. Trace-element geochemistry of mantle olivine and application to mantle petrogenesis and geothermobarometry. *Chem. Geol.* 270, 196–215. <https://doi.org/10.1016/j.chemgeo.2009.11.017>.
- Demouchy, S., Jacobsen, S.D., Gaillard, F., Stern, C.R., 2006. Rapid magma ascent recorded by water diffusion profiles in mantle olivine. *Geology* 34 (6), 429–432. <https://doi.org/10.1130/G22386.1>.
- Dohmen, R., Chakraborty, S., 2007a. Fe–Mg diffusion in olivine II: point defect chemistry, change of diffusion mechanisms and a model for calculation of diffusion coefficients in natural olivine. *Phys. Chem. Miner.* 34 (6), 409–430. <https://doi.org/10.1007/s00269-007-0158-6>.
- Dohmen, R., Chakraborty, S., 2007b. Erratum on “Fe–Mg diffusion in olivine II: point defect chemistry, change of diffusion mechanisms and a model for calculation of diffusion coefficients in natural olivine”. *Phys. Chem. Miner.* 34, 597–598. <https://doi.org/10.1007/s00269-007-0185-3>.
- Dohmen, R., Kasemann, S.A., Coogan, L., Chakraborty, S., 2010. Diffusion of Li in olivine. Part I: experimental observations and a multi species diffusion model. *Geochim. Cosmochim. Acta* 74, 274–292. <https://doi.org/10.1016/j.gca.2009.10.1016>.
- Edmonds, M., 2015. Partitioning of light lithophile elements during basalt eruptions on Earth and application to Martian shergottites. *Earth Planet. Sci. Lett.* 411, 142–150. <https://doi.org/10.1016/j.epsl.2014.11.034>.
- Ferguson, D.J., Gonnermann, H.M., Ruprecht, P., Plank, T., Hauri, E.H., Houghton, B.F., Swanson, D.A., 2016. Magma decompression rates during explosive eruptions of Kilauea volcano, Hawaii, recorded by melt embayments. *Bull. Volcanol.* 78 (71), 1–12. <https://doi.org/10.1007/s00445-016-1064-x>.
- Garcia, M.O., Mucek, A., Lynn, K.J., Swanson, D.A., Norman, M., 2018. Geochemical evolution of Keanakāko'i Tephra, Kilauea Volcano, Hawai'i. In: Poland, M., Garcia, M., Camp, V., Grunder, A. (Eds.), *A Tribute to the Distinguished Career of Don Swanson*. In: *GSA Special Pap.*, vol. 536, in press.
- Garcia, M.O., Pietruszka, A.J., Rhodes, J.M., 2003. A petrologic perspective of Kilauea Volcano's summit magma reservoir. *J. Petrol.* 44 (12), 2313–2339. <https://doi.org/10.1093/ptrology/egg079>.
- Grant, K.J., Wood, B.J., 2010. Experimental study of the incorporation of Li, Sc, Al, and other trace elements into olivine. *Geochim. Cosmochim. Acta* 74, 2412–2428. <https://doi.org/10.1016/j.gca.2010.01.015>.
- Helz, R.T., Clague, D.A., Mastin, L.G., Rose, T.R., 2015. Evidence for large compositional ranges in coeval melts erupted from Kilauea's summit reservoir. In: Carey, R., Cayol, V., Poland, M., Weis, D. (Eds.), *Hawaiian Volcanoes: From Source to Surface*. In: *Geophys. Monogr. Ser.*, vol. 208, pp. 125–145.
- Helz, R.T., Thornber, C.R., 1987. Geothermometry of Kilauea Iki lava lake Hawaii. *Bull. Volcanol.* 49, 651–688.
- Holzappel, C., Chakraborty, S., Rubie, D.C., Frost, D.J., 2007. Effect of pressure on Fe–Mg, Ni, and Mn diffusion in (Fe_xMg_{1-x})₂SiO₄ olivine. *Phys. Earth Planet. Inter.* 162, 186–198. <https://doi.org/10.1016/j.pepi.2007.04.009>.
- Hon, K., Kauhikaua, J., Denlinger, R., Mackay, K., 1994. Emplacement and inflation of pahoehoe sheet flows: observations and measurements of active lava flows on Kilauea Volcano, Hawaii. *Geol. Soc. Am. Bull.* 106, 351–370.
- Ito, M., Ganguly, J., 2006. Diffusion kinetics of Cr in olivine and ⁵³Mn–⁵³Cr thermochronology of early solar system objects. *Geochim. Cosmochim. Acta* 70, 799–809. <https://doi.org/10.1016/j.gca.2005.09.020>.
- Jochum, K.P., Weis, U., Stoll, B., Kuzmin, D., Qichao, Y., Raczek, I., Jacob, D.E., Stracke, A., Birbaum, K., Frick, D.A., Günther, D., Enzweiler, J., 2011. Determination of reference values for NIST SRM 610–617 glasses following ISO guidelines. *Geostand. Geanal. Res.* 35 (4), 397–429. <https://doi.org/10.1111/j.1751-908X.2011.00120.x>.
- Jochum, K.P., Weis, U., Schwager, B., Stoll, B., Wilson, S.A., Haug, G.H., Andreae, M.O., Enzweiler, J., 2016. Reference values following ISO guidelines for frequently requested rock reference materials. *Geostand. Geanal. Res.* 40 (3), 333–350. <https://doi.org/10.1111/j.1751-908X.2015.00392.x>.
- Johnson, D.J., 1992. Dynamics of magma storage in the summit reservoir of Kilauea Volcano, Hawaii. *J. Geophys. Res.* 97 (B2), 1807–1820.
- Jollands, M.C., O'Neill, H.S.C., Van Orman, J., Berry, A.J., Hermann, J., Newville, M., Lanzirotti, A., 2018. Substitution and diffusion of Cr²⁺ and Cr³⁺ in synthetic forsterite and natural olivine at 1200–1500 °C and 1 bar. *Geochim. Cosmochim. Acta* 220, 407–428.
- Kahl, M., Chakraborty, S., Costa, F., Pompilio, M., 2011. Dynamic plumbing system beneath volcanoes revealed by kinetic modeling, and the connection to monitoring data: an example from Mt. Etna. *Earth Planet. Sci. Lett.* 308, 11–22. <https://doi.org/10.1016/j.epsl.2011.05.008>.
- Klein, F.W., Koyanagi, R.Y., Nakata, J.S., Tanigawa, W.R., 1987. The seismicity of Kilauea's magma system. In: *U. S. Geol. Surv. Prof. Pap.*, vol. 1350, pp. 1019–1185.
- Lloyd, A.S., Ruprecht, P., Hauri, E.H., Rose, W., Gonnermann, H.M., Plank, T., 2014. NanoSIMS results from olivine-hosted melt embayments: magma ascent rate during explosive basaltic eruptions. *J. Volcanol. Geotherm. Res.* 283, 1–18. <https://doi.org/10.1016/j.jvolgeores.2014.06.002>.
- Lynn, K.J., Garcia, M.O., Shea, T., Costa, F., 2017. Timescales of mixing and storage for Keanakāko'i Tephra magmas (1500–1823 C.E.), Kilauea Volcano, Hawai'i. *Contrib. Mineral. Petrol.* 172, 76. <https://doi.org/10.1007/s00410-017-1395-4>.
- Matzen, A.K., Baker, M.B., Beckett, J.R., Stolper, E.M., 2011. Fe–Mg partitioning between olivine and high-magnesian melts and the nature of Hawaiian parental liquids. *J. Petrol.* 52, 1243–1263. <https://doi.org/10.1093/ptrology/egq089>.
- National Academies of Sciences, Engineering, and Medicine, 2017. *Volcanic Eruptions and Their Repose, Unrest, Precursors, and Timing*. The National Academies Press, Washington, DC.
- Parkinson, I.J., Hammond, S.J., James, R.H., Rogers, N.W., 2007. High-temperature lithium isotopic fractionation: insights from lithium isotope diffusion in magmatic systems. *Earth Planet. Sci. Lett.* 257, 609–621. <https://doi.org/10.1016/j.epsl.2007.03.023>.
- Patanè, D., Aiuppa, A., Aloisi, M., Behncke, B., Cannata, A., Coltelli, M., Grazia, G.D., Gambino, S., Gurrieri, S., Mattia, M., Salerno, G., 2013. Insights into magma and fluid transfer at Mount Etna by a multiparametric approach: a model of the events leading to the 2011 eruptive cycle. *J. Geophys. Res., Solid Earth* 118, 3519–3539. <https://doi.org/10.1002/jgrb.50248>.
- Paton, C., Hellstrom, J., Paul, B., Woodhead, J., Hergt, J., 2011. Iolite: freeware for the visualization and processing of mass spectrometric data. *J. Anal. At. Spectrom.* 26, 2508–2518. <https://doi.org/10.1039/c1ja10172b>.
- Petry, C., Chakraborty, S., Palme, H., 2004. Experimental determination of Ni diffusion coefficients in olivine and their dependence on temperature, composition, oxygen fugacity, and crystallographic orientation. *Geochim. Cosmochim. Acta* 68 (20), 4179–4188. <https://doi.org/10.1016/j.gca.2004.02.024>.
- Pietruszka, A.J., Heaton, D.E., Marske, J.P., Garcia, M.O., 2015. Two magma bodies beneath the summit of Kilauea Volcano by isotopically distinct melt deliveries

- from the mantle. *Earth Planet. Sci. Lett.* 413, 90–100. <https://doi.org/10.1016/j.epsl.2014.12.040>.
- Poland, M.P., Miklius, A., Montgomery-Brown, E.K., 2014. Magma supply, storage, and transport at shield-stage Hawaiian volcanoes. In: Poland, M.P., Takahashi, T.J., Landowski, C.M. (Eds.), *Characteristics of Hawaiian Volcanos*. In: USGS Prof. Pap., vol. 1801, pp. 179–234.
- Richter, F., Chaussidon, M., Watson, E.B., Mendybaev, R., Homolova, V., 2017. Lithium isotope fractionation by diffusion in minerals Part 2: olivine. *Geochim. Cosmochim. Acta* 219, 124–142. <https://doi.org/10.1016/j.gca.2017.09.001>.
- Rubin, A.E., Cooper, K.M., Till, C.B., Kent, A.J.R., Costa, F., Bose, M., Gravley, D., Deering, C., Cole, J., 2017. Rapid cooling and cold storage in a silicic magma reservoir recorded in individual crystals. *Science* 356, 1154–1156. <https://doi.org/10.1126/science.aam8720>.
- Ruprecht, P., Plank, T., 2013. Feeding andesitic eruptions with a high-speed connection from the mantle. *Nature* 500 (7460), 68–72. <https://doi.org/10.1038/nature12342>.
- Seitz, H., Woodland, A.B., 2000. The distribution of lithium in peridotitic and pyroxenite mantle lithologies – an indicator of magmatic and metasomatic processes. *Chem. Geol.* 166, 47–64.
- Shea, T., Lynn, K.J., Garcia, M.O., 2015a. Cracking the olivine zoning code: distinguishing between crystal growth and diffusion. *Geology* 43 (10), 935–938. <https://doi.org/10.1130/G37082.1>.
- Shea, T., Costa, F., Krimer, D., Hammer, J.E., 2015b. Accuracy of timescales retrieved from diffusion modeling in olivine: a 3D perspective. *Am. Mineral.* 100, 2026–2042. <https://doi.org/10.2138/am-2015-5163>.
- Sides, I.R., Edmonds, M., MacLennan, J., Swanson, D.A., Houghton, B.F., 2014. Eruption style at Kilauea Volcano in Hawai'i linked to primary melt composition. *Nat. Geosci.* 7, 464–469. <https://doi.org/10.1038/ngeo2140>.
- Sparks, S.R.J., Sigurdsson, H., Wilson, L., 1977. Magma mixing: a mechanism for triggering acid explosive eruptions. *Nature* 267, 315–318. <https://doi.org/10.1038/267315a0>.
- Swanson, D.A., Houghton, B.F., 2018. Products, processes, and implications of Keanakāko'i volcanism, Kilauea Volcano, Hawai'i. In: Poland, M., Garcia, M., Camp, V., Gruner, A. (Eds.), *A Tribute to the Distinguished Career of Don Swanson*. In: *GSA Special Pap.*, vol. 536, in press.
- Swanson, D.A., Rose, T.R., Mucek, A.E., Garcia, M.O., Fiske, R.S., Mastin, L.G., 2014. Cycles of explosive and effusive eruptions at Kilauea Volcano, Hawai'i. *Geology* 42 (7), 631–634. <https://doi.org/10.1130/G35701.1>.
- Swanson, D.A., Rose, T.R., Fiske, R.S., McGeehin, J.P., 2012. Keanakāko'i Tephra produced by 300 years of explosive eruptions following collapse of Kilauea's caldera in about 1500 CE. *J. Volcanol. Geotherm. Res.* 215–216, 8–25. <https://doi.org/10.1016/j.jvolgeores.2011.11.009>.
- Tang, M., Rudnick, R.L., McDonough, W.F., Bose, M., Goreva, Y., 2017. Multi-mode Li diffusion in natural zircons: evidence for diffusion in the presence of step-function concentration boundaries. *Earth Planet. Sci. Lett.* 474, 110–119. <https://doi.org/10.1016/j.epsl.2017.06.034>.
- Tomascak, P.B., Magna, T., Dohmen, R., 2016. *Advances in Lithium Isotope Geochemistry*. Springer International Publishing, Switzerland, 195 pp.
- Vlastélic, I., Staudacher, T., Bachélery, P., Télouk, P., Neuville, D., Benbakkar, M., 2011. Lithium isotopic fractionation during magma degassing: constrains from silicic differentiates and natural gas condensates from Piton de la Fournaise volcano (Réunion Island). *Chem. Geol.* 284, 26–34. <https://doi.org/10.1016/j.chemgeo.2011.02.002>.
- Watson, E.B., Cherniak, D.J., Holycross, M.E., 2015. Diffusion of phosphorus in olivine and molten basalt. *Am. Mineral.* 100, 2053–2065. <https://doi.org/10.2138/am-2015-5416>.
- Weyer, S., Seitz, H.M., 2012. Coupled lithium- and iron isotope fractionation during magmatic differentiation. *Chem. Geol.* 294–295, 42–50. <https://doi.org/10.1016/j.chemgeo.2011.11.020>.
- Wilson, C.J.N., Morgan, D.J., Charlier, B.L.A., Barker, S.J., 2017. Comment on “Rapid cooling and cold storage in a silicic magma reservoir recorded in individual crystals”. *Science* 358, eaap8429. <https://doi.org/10.1126/science.aap8429>.
- Wright, T.L., Fiske, R.S., 1971. Origin of the differentiated and hybrid lavas of Kilauea Volcano, Hawaii. *J. Petrol.* 12 (1), 1–65. <https://doi.org/10.1093/petrology/12.1.1>.